Proc. Natl. Acad. Sci. USA
Vol. 78, No. 5, pp. 2952–2956, May 1981
Biophysics

Oscillations and control features in glycolysis: Numerical analysis of a comprehensive model

(phosphofructokinase-pyruvate kinase reaction coupling/efficiency/ATP/ADP ratio)

YVES TERMONIA AND JOHN ROSS

Department of Chemistry, Stanford University, Stanford, California 94305

Contributed by John Ross, January 23, 1981

ABSTRACT **We present an analysis of glycolysis based on experimental findings and an interpretation based on concepts of efficiency, resonance response, and control features available in highly nonlinear reaction kinetics. We begin with a model for the glycolytic mechanism that is comprehensive, includes a large number of known activations and inhibitions of enzymes by metabolites, and couples the phosphofructokinase (PFKase) and the pyruvate kinase (PKase) reactions. The PFKase and PKase reactions and the coupling between them are modeled according to experimental information, but we do not attempt to model the glyceraldehyde-3-phosphate dehydrogenase-3-phosphoglycerate kinase reaction. We use experimental data to obtain the best estimates for the kinetic parameters and test the model by calculating the concentration variations of the intermediate metabolites. We confirm oscillatory behavior and calculate the ATP/ADP ratio and the free-energy dissipation for an extended range of the kinetic parameters as a function of the driving force for the glycolytic pathway, a measure of which is the total adenine nucleotide concentration. We find agreement of the calculated results with experimental findings except for the insufficiently represented reactions. Our model shows that the average ATP/ADP ratio is increased and the average free-energy dissipation is decreased in an oscillatory compared with a steady state mode of operation. The average values of the ATP/ADP ratio and of the free energy dissipation change abruptly past the onset of sustained oscillations.**

Glycolytic oscillations were first observed in intact yeast cells and yeast cell extracts and, later, also in beef heart extract (for review, see ref. 1). There arises the question of the purpose, if any, of oscillations of concentrations in glycolysis. Recently, Richter and Ross (2) suggested that the efficiency of energy transfer, related to the entropy production, is variable and may be higher in an oscillatory compared with a steady-state mode of operation. These features arise from the possibility of a resonance response of the pyruvate kinase PKase reaction to the phosphofructokinase PFKase reaction. They have the advantages of control and efficiency and may thus have been incorporated in the evolutionary development of glycolysis.

We present an analysis and interpretation of glycolysis closely based on experimental findings and an interpretation based on concepts of efficiency and resonance response. We begin with a model for the glycolytic mechanism that is comprehensive (for comparison, see refs. 3–5) and includes a large number of known activations and inhibitions of enzymes by metabolites. The PFKase and the PKase reactions are coupled, but we do not attempt to model the glyceraldehyde-3-phosphate dehydrogenase-3-phosphoglycerate kinase (GAPDHase/PGKase) reactions. Next, we extract from experimental data the best estimates for the kinetic parameters. We then test the model by calculating the concentration variations of the intermediate metabolites and find oscillatory behavior. We further calculate the ATP/ADP ratio and the free energy dissipation in an extended range of the kinetic parameters as a function of the driving force for the glycolytic pathway, a measure of which is the total adenine nucleotide concentration [A(MDT)P]. We find substantial agreement of the calculated results with experimental findings, except for the insufficiently represented (GAPDHase/PGKase) reactions. Our model shows that the average ATP/ADP ratio is increased and the average free-energy dissipation is decreased in an oscillatory compared with a steady-state mode of operation. Furthermore, the average values of the ATP/ADP ratio and of the free-energy dissipation change abruptly past the onset of sustained oscillations.

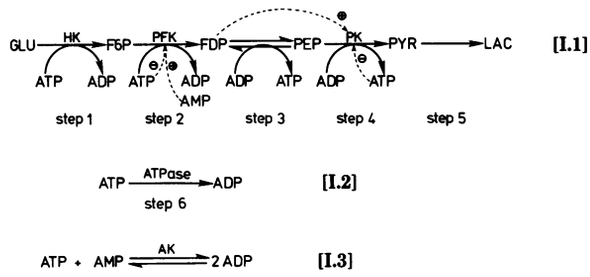

FIG. 1. Model for glycolysis. Arrows in one direction only indicate almost irreversible reactions. Arrows in both directions indicate reactions close to equilibrium. Broken lines indicate activation (⊕) or inhibition (⊖) of enzymes by metabolites, which are taken into account in the model. GLU, Glc; HK, HKase; F6P, Fru-6-*P*; PFK, PFKase; FDP, Fru-1,6-P_2, PEP, *P-e*-Prv; PK, PKase; PYR, Prv; AK, AKase.

MODEL

Description. Fig. 1 shows the scheme for our model of the glycolytic pathway that converts glucose into lactic acid. The scheme includes the ATPase reaction **I.2** and the adenylate kinase (AKase) reaction [**I.3**]. The reaction sequence (Eq. **I.1**) includes the PFKase and the PKase reactions, which are (with the HKase reaction) the most irreversible steps in the pathway and believed to have important regulatory functions (6). [The standard free-energy changes (ΔG^0) are −3.42, −3.4, and −11.44 kcal/mol (1 cal = 4.18 J) for the HKase, PFKase, and PKase reactions, respectively.] The most important interactions of metabolites with enzymes are included in the model: ATPase inhibition and AMPase activation of PFKase (5, 7, 9)*; fructose

The publication costs of this article were defrayed in part by page charge payment. This article must therefore be hereby marked "*advertisement*" in accordance with 18 U. S. C. §1734 solely to indicate this fact.

Abbreviations: Glc, glucose; Glc-6-*P*, glucose 6-phosphate; Fru-6-*P*, fructose 6-phosphate; Fru-1,6-P_2, fructose 1,6-bisphosphate; *P-e*-Prv, phospho*enol*pyruvate; Prv, pyruvate; A(MDT)P, total adenine nucleotides; LAC, lactic acid; HKase, hexokinase; PFKase, phosphofructokinase; GAPDHase, glyceraldehyde-3-phosphate dehydrogenase; PGKase, 3-phosphoglycerate kinase; PKase, pyruvate kinase; AKase, adenylate kinase; MWC, Monod, Wyman, and Changeux.

* In yeast cells and extracts, there is no activation of PFKase by Fru-1,6-P_2, because the concentration of Fru-1,6-P_2 remains too high throughout the oscillation period (5). Only in muscle is PFKase activated by Fru-1,6-P_2.

1,6-bisphosphate (Fru-1,6-P_2) activation of PK (5, 6, 9, 10)†; ATPase inhibition of PKase (9, 10).

In deriving the above scheme, we made the following simplifications suggested by experimental evidence: (*i*) The reaction catalyzed by glucose-phosphate isomerase, which converts glucose 6-phosphate (Glc-6-*P*) into Fru-6-*P*, is at equilibrium (5, 7). This is justified by two considerations—the rapidity of the reaction and the low relaxation time of the PFKase, which mainly determines the relaxation times of Glc-6-*P* and Fru-6-*P* (7). (*ii*) We have lumped all the intermediate (reversible) reactions between Fru-1,6-P_2 and *P-e*-Prv into an overall reversible reaction [topological contraction (7)] even though the intermediate PGKase reaction has $\Delta G > RT$ (6). That reaction has not thus far been assigned regulatory functions (6) and, for this study, we therefore lump it together with the other reversible steps. (*iii*) The AKase reaction is at equilibrium because it is very fast (5, 7). (*iv*) The total adenine nucleotide concentration is nearly constant because of the slowness of the processes that change it (13). For simplicity and without any loss of generality, we make the additional following assumptions: (*v*) The HKase reaction operates at a constant rate (5). We thus neglect the inhibition of HKase by Glc-6-*P* and its dependence on the concentration in the cosubstrate ATP. Changes in the HKase rate would have some influence on the PFKase rate, but these would not alter the basic oscillatory process. We have checked this by computer calculations, assuming a Michaelis–Menten dependence of the HKase rate on the ATP concentration. (*vi*) The concentrations in glucose (Glc) and lactic acid (LAC) are constant.

Rate Equations. *Step 1*. The flow is constant and denoted by *V*.

Step 2. The fully concerted model of Monod, Wyman, and Changeux (MWC) has been extensively used for the study of the PFKase reaction (3, 12, 13). That model is convenient for our purposes because all its parameters can be determined from experimental data. We thus make the usual MWC assumptions for the PFKase enzyme (for review and discussion of enzyme kinetic models, see ref. 14). (*i*) The enzyme is a perfect *K* system—i.e., one in which the kinetic parameter V^m (saturation or maximum velocity) is invariant. (*ii*) The enzyme is assumed to be an oligomer, made up of *n* equivalent and independent subunits (protomers) each of which bears a single site for each of the stereospecific ligands. (*iii*) The protomer may exist in two different conformational states considered to be in equilibrium: an active state (*R*) and an inactive state (*T*). The equilibrium between the *R* and *T* states is a function of the concentration of all the effectors (inhibitors and activators) and not of the substrate. (*iv*) The transitions between the *R* and *T* states are supposed to be "fully concerted." In other words, PFKase may exist in only two forms: one ($PFKase_R$) containing *n* active protomers and the other ($PFKase_T$) containing *n* inactive protomers.

All models for cooperative substrate binding lead to a typical curve for the dependence of the enzyme velocity on the substrate concentration. These curves can be fitted in most cases by a simple expression of the so-called Hill form. That simple form can be obtained from the MWC model if one further assumes that (*v*) the substrate binds exclusively to the active form ($PFKase_R$) of the enzyme (this corresponds to the limit $c = 0$ in the MWC model) and (*vi*) all the ligands (effectors and substrate) are bound to the enzyme in virtually a single step, which implies that the cooperativity reaches an extreme.

Thus, the mechanism for step 2 may be stated as

$$n\ \text{Fru-6-}P + \text{PFKase}_R \underset{\bar{s}_1}{\overset{s_1}{\rightleftharpoons}} [\text{PFKase}\cdot\text{Fru-6-}P^n] \qquad \text{[II.1]}$$

$$[\text{PFKase}\cdot\text{Fru-6-}P^n] \xrightarrow{s_2} n\ \text{Fru-1,6-}P_2 + \text{PFKase}_R$$

with, in addition, the activation-inhibition reaction

$$n\ \text{ATP} + \text{PFKase}_R \underset{\bar{s}_3}{\overset{s_3}{\rightleftharpoons}} \text{PFKase}_T + n\ \text{AMP}, \qquad \text{[II.2]}$$

which determines the equilibrium constant between the *R* and *T* forms of the enzyme.‡ Mechanism II satisfies the rate law

$$V_2 = V_2^m\,[\text{Fru-6-}P]^n \Big/ \left(K_2 + K_2R_2\frac{[\text{ATP}]^n}{[\text{AMP}]^n} + [\text{Fru-6-}P]^n\right) \qquad [1]$$

where $V_2^m = s_2[\text{PFKase}]$, $K_2 = (s_2 + \bar{s}_1)/s_1$, and $R_2 = s_3/\bar{s}_3$. In deriving Eq. 1, the assumption has been made that the enzyme concentrations are stationary. The validity of that assumption has been demonstrated by Heinrich and Rapoport (7). Because the *n* protomers are independent, we have

$$R_2 = (K_R^{\text{AMP}}/K_T^{\text{ATP}})^n, \qquad [2]$$

where K_R^{AMP} is the dissociation constant for the activator AMP bound to the *R* conformation of the enzyme and K_T^{ATP} is the dissociation constant for the inhibitor ATP bound to the *T* conformation. We also have

$$K_2 = (K_2^m)^n, \qquad [3]$$

where K_2^m is the Michaelis–Menten constant for the substrate Fru-6-*P*.

Step 3. The flow for this step is assumed to be of the form

$$V_3 = k_3[\text{Fru-1,6-}P_2]^\alpha - \bar{k}_3[P\text{-}e\text{-Prv}]^\beta. \qquad [4]$$

The parameters (k_3, α) and $(\bar{k}_3, \beta)$ are determined from experimental values of the average forward and backward fluxes for the actual pathway represented by step 3.

Step 4. The allosteric MWC model has been also used (3, 9) to analyze the kinetics of pyruvate kinase (PKase). We thus make the same assumptions for the PKase reaction as for the PFKase reaction. The flow for step 3 has the form

$$V_4 = V_4^m[P\text{-}e\text{-Prv}]^\gamma \Big/ \left(K_4 + K_4R_4\frac{[\text{ATP}]^m}{[\text{Fru-1,6-}P_2]^m} + [P\text{-}e\text{-Prv}]^\gamma\right), \quad [5]$$

where, for Eq. **5** to be consistent with experimental evidence (see below), we have assumed that the number of ligand molecules that bind to one molecule of the enzyme depends on the type of ligand. In Eq. **5**, we have

$$R_4 = (K_R^{\text{Fru-1,6-}P_2}/K_T^{\text{ATP}})^m, \qquad [6]$$

where K_R and K_T are dissociation constants for ligands bound to the *R* and *T* conformations of PKase, respectively. We also have

$$K_4 = (K_4^m)^\gamma, \qquad [7]$$

where K_4^m is the Michaelis–Menten constant for the substrate *P-e*-Prv.

Step 5. The rate of removal of Prv is assumed to be of the form

$$V_5 = -k_5[\text{Prv}]. \qquad [8]$$

† In yeast, heart, and liver, PKase activity is dependent on Fru-1,6-P_2, whereas in skeletal muscle it is not (5).

‡ Our choice of an activation-inhibition reaction of the type **II.2**, first suggested by Higgins (15), avoids the consideration usually made in the MWC model of the existence of an allosteric constant L_0 in the absence of effectors. Also, the determination, from experiment, of the dissociation constants K_R^{AMP} and K_T^{ATP} of the MWC model (see Eq. **2**) is independent of the choice of L_0.

Table 1. Best estimates of kinetic parameters

	Parameter	Experimental data: Value	Experimental data: Origin	Best estimate
Step 1	V	0.33–2.66 mM/min	Yeast (12)	2 mM/min
Step 2	V/V_2^m	0.16	Yeast (16)	Same as experimental data
	n	2	Muscle (17); MWC model (3, 12)	Same as experimental data
	K_2^m	0.04 mM	Brain (18)	Same as experimental data
	K_R^{AMP}	25 μM*	MWC model applied to *Escherichia coli* (13)	Same as experimental data
	K_T^{ATP}	60 μM	MWC model applied to *E. Coli* (13)	Same as experimental data
Step 3	k_3	Not available		5.8/min†
	α	Not available		0.05†
	$\bar{k}_3$	Not available		0.01/min†
	β	Not available		6†
Step 4	V/V_4^m	0.02	Yeast (16)	Same as experimental data
	γ	1	*Saccharomyces carlsbergensis*‡ (9)	Same as experimental data
	m	4	*S. carlsbergensis*‡ (9)	Same as experimental data
	K_4^m	0.6 mM	Liver (20)	Same as experimental data
	K_T^{ATP}	9.3 mM ± 8.1%	MWC model applied to *S. carlsbergensis* (9)	Same as experimental data
	$K_R^{Fru\text{-}1,6\text{-}P_2}$	0.2 mM ± 4.7%	MWC model applied to *S. carlsbergensis* (9)	Same as experimental data
Step 6	k_6	0.1/min	Rat erythrocytes (7)	Same as experimental data
AKase reaction	K	1	Skeletal muscle (5)	Same as experimental data
Step 5	k_5	Not available		1/min

* The value is actually for ADP.
† See text.
‡ *P-e*-Prv saturation curves give $\gamma = 1$–2.45. A value of $\gamma = 1$ has also been obtained in liver (19). Data on the binding of Fru-1,6-P_2 to PKase give 4 protomers per mol.

Because the concentration of Prv does not affect the kinetics of the PFKase and PKase reactions, the choice of a value for k_5 is immaterial.

Step 6. We put

$$V_6 = -k_6[\text{ATP}], \quad [9]$$

where k_6 is determined experimentally from the slope of the ATPase rate versus the ATP concentration in the linear region.

Steady State. The steady-state concentrations of the various metabolites—Fru-6-*P*, Fru-1,6-P_2, *P-e*-Prv, Prv, ATP, ADP, and AMP are obtained from the system of equations

$$\frac{d[\text{Fru-6-}P]}{dt} = V - V_2 = 0 \quad [10]$$

$$\frac{d[\text{Fru-1,6-}P_2]}{dt} = V_2 - V_3 = 0 \quad [11]$$

$$\frac{d[P\text{-}e\text{-Prv}]}{dt} = 2V_3 - V_4 = 0 \quad [12]$$

$$\frac{d[\text{Prv}]}{dt} = V_4 - V_5 = 0 \quad [13]$$

$$\frac{d[\text{ATP}]}{dt} = -V - V_2 + 2V_3 + V_4 - V_6 = 0 \quad [14]$$

$$\frac{[\text{ATP}][\text{AMP}]}{[\text{ADP}]^2} = K \quad [15]$$

$$[\text{ATP}] + [\text{ADP}] + [\text{AMP}] = [\text{A(MDT)P}]. \quad [16]$$

The factor 2, which multiplies V_3 in Eqs. **12** and **14**, comes from the fact that two moles each of *P-e*-Prv and ATP are produced each time one mole of Fru-1,6-P_2 is consumed. The constant K in Eq. **15** is the equilibrium constant for the AKase reaction. Eq. **16** expresses the conservation of adenine nucleotides.

Determination from Experimental Data of the Best Estimates for the Kinetic Parameters. Table 1 lists the best estimates for the kinetic parameters, as extracted from experimental data. The determination of the parameters for step 3 requires some justification. Experimental data on Ehrlich ascites tumor cells (6) show that the average forward flux for the actual pathway represented by step 3 is ≈2.9 times the input flow V. If we choose α small ($\alpha = 0.05$), so that the forward flux for step 3 is only weakly dependent on the concentration of Fru-1,6-P_2, the experimental data suggest that $k_3 = 5.8$/min. With that choice, results for our model show that almost any couple of values for the parameters $\bar{k}_3$ and β leads to a reverse flux of ≈1.7 times V. That factor is close to the value 1.5 found experimentally in Ehrlich ascites tumor cells (6). Our choice of a relatively large value of β ($\beta = 6$) is guided by the following consideration. When β is large and α is small, step 3 plays the role of a feedback regulator for the concentration of *P-e*-Prv: any increase in the concentration of *P-e*-Prv decreases the input flow

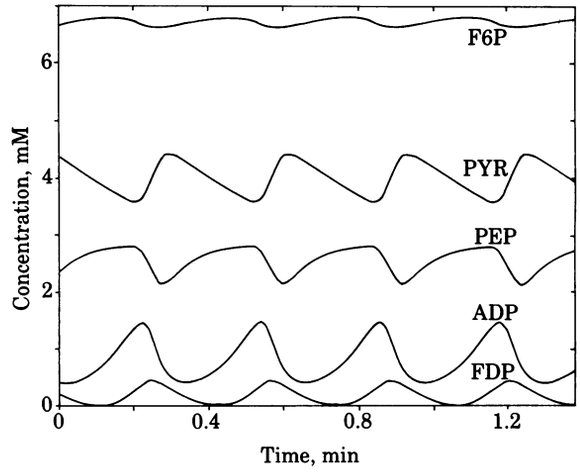

FIG. 2. Time dependence of the concentrations of Fru-6-*P*, Fru-1,6-P_2, *P-e*-Prv, Prv, and ADP as calculated from the model. (Concentrations of Glc and LAC were assumed to be constant.) The figure shows four oscillation periods. The concentration of Fru-6-*P* has been reduced by a factor of two. Abbreviations are as given in the legend to Fig. 1.

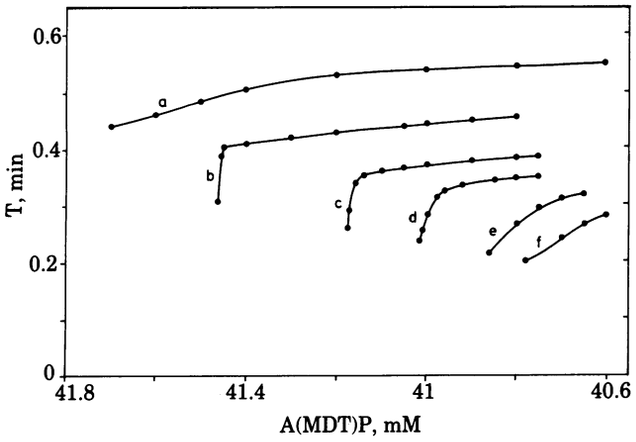

FIG. 3. Dependence of T on A(MDT)P concentration. The points are calculated, and the curve is drawn to connect the points. The figure is for different values of k_3. The points of marginal stability are the ones on the extreme left of each curve. Curves: a, $k_3 = 2.2$; *b*, $k_3 = 4$; c, $k_3 = 5$; *d*, $k_3 = 5.8$; *e*, $k_3 = 7$; *f*, $k_3 = 8$.

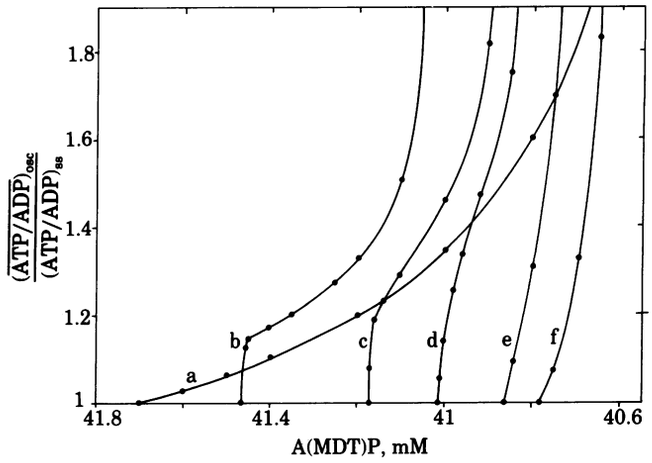

FIG. 4. Dependence of $\overline{(ATP/ADP)}_{osc}$ on A(MDT)P concentration. The values were obtained by averaging over one period of the oscillations, and they are given in units of the steady-state ratio $(ATP/ADP)_{ss}$. The curves correspond to those shown in Fig. 3.

of it and vice versa. The presence of such a regulation of the *P-e*-Prv concentration is substantiated by the observation that *P-e*-Prv acts as a feedback inhibitor of PFKase (13).

It is important to stress that the parameter values listed in Table 1 are only for the purpose of comparison of our model to experiment. The numerical results presented below cover a wider range of values of these parameters.

RESULTS AND DISCUSSION

In this section we present computational time-dependent solutions of the model for the glycolytic pathway shown in Fig. 1. Straightforward numerical integration of these solutions gives the dependence of the average ATP/ADP ratio and free-energy dissipation on the driving force for the pathway, a measure of which is the A(MDT)P concentration. We then compare, when possible, our calculated results with experimental values.

The time-dependent solutions of our model have been obtained by numerical integration of Eqs. **10–14** by fourth-order Runge–Kutta method. We start with the (unstable) stationary system, which is then perturbed by decreasing the ATP concentration by 1%. We compute 100 oscillations in the concentrations, each oscillation being described by 40 points. The period T of the oscillations is estimated from the time that separates the last two minima of equal amplitude in the ATP concentration. An illustration of the oscillatory behavior obtained in this way is given in Fig. 2. The values of the parameters are the best estimates extracted from experimental data and given in Table 1 and the concentration of adenine nucleotides is 40.95 mM.

Fig. 3 gives the dependence of T of the self-sustained oscillations on the total adenine nucleotide concentration A(MDT)P. The figure is for different values of k_3, which represents the forward rate constant for step 3. The value $k_3 = 5.8$ is that suggested from experimental findings. The values of the other parameters are the best estimates as given in Table 1. Because the stationary concentration of ATP is constant for the figure, a decrease in A(MDT)P concentration corresponds to an increase in the stationary ATP/ADP ratio and vice versa. As the A(MDT)P concentration is decreased from 41.7 to 40.6, the stationary ATP/ADP ratio is increased from 24.5 to 67.6. The parameter A(MDT)P thus plays the role of a pump parameter for the generation of self-sustained oscillations. The points of marginal stability, for which the amplitudes of the oscillations are very small, are the first ones on the extreme left of each curve.

Inspection of Fig. 3 shows that, for low values of k_3 ($k_3 = 2.2$, see curve a), T increases monotonically as the distance from marginal stability is increased [A(MDT)P is decreased]. For larger values of k_3, however, the T curves change abruptly past the onset of self-sustained oscillations. The curves subsequently level off at a given value of T, depending on k_3. Inspection of Fig. 3 also shows that the changes in the T curves become less abrupt as k_3 is further increased. Still (see curve f, for example), T increases by as much as 40% as A(MDT)P is varied by less than 2 mM (compare with curve a).

Fig. 4 gives the dependence of the average oscillatory ratio $\overline{(ATP/ADP)}_{osc}$ on the A(MDT)P concentration. The curves correspond to the parameters of those given in Fig. 3. The values are in units of the corresponding (unstable) steady-state ratio. As a general result, we observe that oscillations always give a higher ATP/ADP ratio. A qualitative experimental verification of that observation has been given by Tornheim (5) for a different system. Perhaps more important is the observation that a very rapid increase in the $\overline{(ATP/ADP)}_{osc}$ ratio occurs in those regions in which the period of the oscillations changes abruptly (Fig. 3). This points to important regulatory functions of the glycolytic oscillations. Because the dependence of the $\overline{(ATP/ADP)}_{osc}$ ratio on the A(MDT)P concentration can be strong near the onset of self-sustained oscillations, a slight variation in A(MDT)P may give rise to an alternative operation of metabolic pathways with ATP-utilizing functions being favored. This may give a cell a very precise way of controlling its metabolic processes. A last remark, we did not observe any significant difference in the average energy charge ratio in a steady-state or oscillatory mode of operation.

The free energy dissipated in the glycolytic pathway is made of two contributions. The first comes from the dissipation in the overall Glc → LAC reaction. That dissipation is simply

$$V(\mu_{Glc} - \mu_{LAC}),$$

which, as μ_{Glc} and μ_{LAC} are held constant, is independent of the regime (stationary or oscillatory) of the intermediate metabolites. The second comes from the overall ADP → ATP reaction. Here, the dissipation is regime dependent. For a stationary regime, that dissipation is

$$D_{ss} = 2V(\mu_{ADP} - \mu_{ATP}), \qquad [17]$$

whereas, for an oscillatory regime, we get an average value

Table 2. Comparison of experimental and calculated properties of the sustained oscillations

Property	Model*	Experiment†
Oscillatory range of substrate input (V)	Finite	Finite
Period (T)	Of the order of min; decreases as V increases	Of the order of min; decreases as V increases
Periodic change in PFKase activity (in % of V_2^m)	Minimum <1; maximum 70; mean 16	Minimum 1; maximum 80; mean 16
Phase shifts	180° for Fru-1,6-P_2 and Fru-6-P, Prv and P-e-Prv, and ADP and ATP	180° for Fru-1,6-P_2 and Fru-6-P, Prv and P-e-Prv, and ADP and ATP
	80–120° for ATP and Fru-1,6-P_2	80–120° for ATP and Fru-1,6-P_2
	210–260° for P-e-Prv and Fru-1,6-P_2	80–120° for P-e-Prv and Fru-1,6-P_2
Periodic change in $(ATP/ADP)_{osc}$ [in % of $(ATP/ADP)_{ss}$]	Minimum 60; maximum 400; mean 100–190 (see Fig. 4)	Minimum 100; maximum 400; mean 266‡

* Except for the oscillatory range of substrate input and for the period, the results presented for our model are for the range of parameter values shown in Figs. 3 and 4.

† Unless otherwise stated, values are those reported in ref. 16.

‡ These results are for an experiment reported in ref. 5.

$$\overline{D}_{osc} = T^{-1} \int_0^T (2V_3 + V_4 - V - V_2)(\mu_{ADP} - \mu_{ATP})dt. \quad [18]$$

Fig. 5 gives the values of $(\overline{D}_{osc} - D_{ss})/|D_{ss}|$ corresponding to the curves given in Fig. 3. As a general result, one observes that oscillations always decrease the dissipation. Again, more important is the observation that the decrease becomes very fast in those regions in which T and $\overline{(ATP/ADP)}_{osc}$ change abruptly (Figs. 3 and 4). This again gives the system important regulatory properties, as already discussed in connection with Fig. 4.

Before comparing our results with experimental findings, it is important to stress that the sometimes sharp transitions observed in Figs. 3–5 are quite general and do not depend on the particular values of the parameters. Results (not reproduced) show that transitions can be obtained for several different sets of values of the parameters of the system, which are totally unrelated to experimental evidence. Furthermore, the presence of these transitions does not depend on the particular type of kinetics chosen for the individual steps in the model. For example, if we make the rates for steps 3 and 4 dependent on the concentration of ADP, the essential features of the model are not affected. To conclude, we believe that the foundation for these transitions lies in the specific structure of the model and its particular pattern of activations and inhibitions.

We now compare the predictions of our model with experimental findings. The steady-state properties of the model are in agreement with experiment (5): concentrations of the intermediate metabolites are in the millimolar range and the ATP/ADP ratio, which varies from 24.5 to 67.6 in Figs. 3–5, lies in the range of experimental observation. The oscillatory properties of the model are compared with experiment in Table 2. Inspection of the table shows that the oscillatory behavior as predicted by our model is in qualitative agreement with experimental findings. The only discrepancy lies in the value of the phase shift between P-e-Prv and Fru-1,6-P_2, which is due to the neglect in our model of the intermediate GAPDHase/PGKase reactions between Fru-1,6-P_2 and P-e-Prv. These reactions indeed lead to an important phase shift between reactants and products, which accounts in part for the discrepancy between our results and experimental data. We did not find any significant dependence of the characteristics presented in Table 2 on the values of the model parameters.

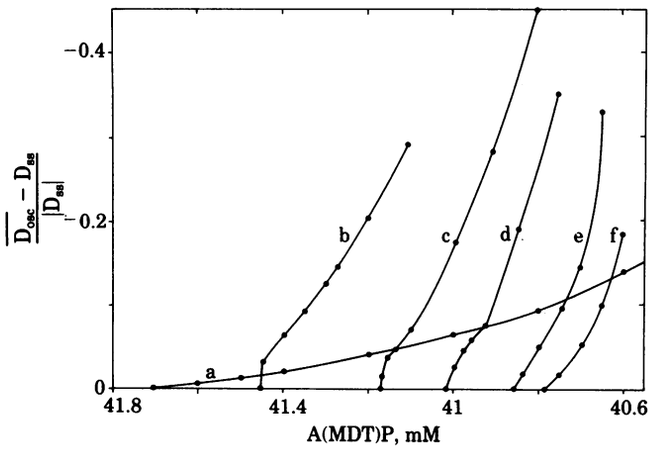

FIG. 5. Dependence of $\overline{D}_{osc}$ in the overall ADP → ATP reaction, on A(MDT)P concentration. The curves correspond to those shown in Fig. 3.

We thank Dr. Peter H. Richter for helpful discussions. This work was supported in part by the National Science Foundation (Y.T.) and the U.S. Department of Energy (J.R.). Y.T. also acknowledges a fellowship from the North Atlantic Treaty Organization for the early part of this work.

1. Hess, B. & Boiteux, A. (1971) *Annu. Rev. Biochem.* **40**, 237–258.
2. Richter, P. H. & Ross, J. (1980) *Biophys. Chem.* **12**, 285–297.
3. Plesser, T. (1977) in *Siebente Internationale Konferenz über Nichtlineare Schwingungen*, ed. Schmidt, G. (Akademie, Berlin), pp. 273–280.
4. Hess, B. & Plesser, T. (1979) *Ann. N.Y. Acad. Sci.* **316**, 203–213.
5. Tornheim, K. (1979) *J. Theor. Biol.* **79**, 491–541.
6. Hess, B. & Brand K. (1965) in *Control of Energy Metabolism*, eds. Chance, B., Estabrook, R. W. & Williamson, J. R. (Academic, New York), pp. 111–122.
7. Heinrich, R. & Rapoport, S. M. (1977) *Prog. Biophys. Mol. Biol.* **32**, 1–82.
8. Frenkel, R. (1968) *Arch. Biochem. Biophys.* **125**, 157–165; 166–174.
9. Johannes, K. J. & Hess, B. (1973) *J. Mol. Biol.* **76**, 181–205.
10. Hess, B. (1975) *Adv. Enzyme Regul.* **14**, 229–241.
11. Lowy, B. A., Ramot, B. & London, I. M. (1958) *Nature (London)* **181**, 324–326.
12. Boiteux, A., Goldbeter, A. & Hess, B. (1975) *Proc. Natl. Acad. Sci, USA* **72**, 3829–3833.
13. Blangy, D., Buc, H. & Monod, J. (1968) *J. Mol. Biol.* **31**, 13–35.
14. Tze Fei Wong, J. (1975) *Kinetics of Enzyme Mechanisms* (Academic, New York).
15. Higgins, J. (1967) *Ind. Eng. Chem.* **59**, 5, 18–62.
16. Hess, B., Boiteux, A. & Kruger, J. (1969) *Adv. Enzyme Regul.* **7**, 149–167.
17. Mahler, H. R. & Cordes, E. H. (1968) *Basic Biological Chemistry* (Harper & Row, New York).
18. Lowry, O. H. & Passonneau, J. V. (1966) *J. Biol. Chem.* **241**, 2268–2279.
19. Carminatti, H., Jiménez de Asúa, L., Recondo, E., Passeron, S. & Rozengurt, E. (1968) *J. Biol. Chem.* **243**, 3051–3056.
20. Rozengurt, E., De Asúa, L. J. & Carminatti, H. (1969) *J. Biol. Chem.* **244**, 3142–3147.